NIPPON STEEL TECHNICAL REPORT No. 89 JANUARY 2004

UDC 669 . 162 . 26 : 681 . 3

Development of Visual Evaluation and Numerical Analysis System of Blast Furnace

–Development of Visual Information Technique of Blast Furnace Process Data–

Masahiro ITO*1 Shinroku MATSUZAKI*1
Kazumoto KAKIUCHI*2 Makoto ISOBE*3

Abstract

The data of the measurement sensor installed with the spatial distribution on the blast furnace were successively accumulated on line from process computer to data base system for a long period of time, the new system which considers the relation with the installation position of each sensor correctly, and carries out picture computerization of the measurement data was developed, and the overall operation state of a blast furnace which the skilled operator could be imagining in each one of heads by experience was visualized as the picture information objectively. Furthermore, as secondary manipulation of visual information, the time differential ratio of stave temperature with a forgetting factor and the spatial differential vector of shaft pressure were newly defined, and the operation surveillance method of the blast furnace which is not before and which visualizes objectively the potential information to measurement data, such as the root of the cohesive zone, was devised.

1. Introduction

Techniques to quantitatively analyze and control the conditions inside a blast furnace have been established thanks to technical advancements such as development of various physical models[1-4] and application of artificial intelligence, or AI[5-10]. In order to further stabilize the operation of a blast furnace, it is necessary further to quantitatively evaluate and analyze non-steady behaviors (dynamic behaviors and characteristics) of phenomena that take place in a bast furnace. As an example of such attempts, a 3-dimensional non-steady physical model[11] is now being developed.

A variety of sensors to directly measure the internal temperature, pressure and other conditions of a blast furnace have been developed, and they have significantly contributed to clarifying what is taking place in a blast furnace. Besides these, various sensors are provided on the shell of a blast furnace for continuous and long-term measurement of temperature, etc., but these sensors measure the conditions inside a furnace only indirectly from outside the shell of a furnace.

Based on experiences accumulated over a long period, a blast furnace operator judges the operating conditions of a furnace by comprehensively evaluating data obtained through the direct furnace inside measurement and indirect shell measurement. Thus, the understanding and prediction especially of non-steady phenomena of a blast furnace depend largely on the experience and skill of furnace operators. In this situation, the authors thought that in order to further stabilize blast furnace operation and decrease the consumption

*1 Environment & Process Technology Center
*2 Kimitsu Works
*3 Oita Works

ratio of reducing agents it would be necessary to develop a technology to quantitatively evaluate the non-steady phenomena of a blast furnace and a modeling technology and a system to flexibly and adequately propose operation guidance based on the quantitative evaluation. As the first step toward this end, they developed the visual evaluation and numerical analysis system of blast furnace as a new technology to integrate and quantitatively evaluate the data from many temperature and pressure sensors provided at various positions of a blast furnace.

The developed system is characterized by a new approach to regard a blast furnace as a process of distributed parameter system having 3-dimensional distribution characteristics and quantify the non-steady behaviors of furnace phenomena from this view point.

Although the measurement data from the various sensors provided on a blast furnace were conventionally input to a process computer, they were not always fully analyzed quantitatively from the above view point and were discarded after a certain time period for reasons such as:

1) There was no hardware or a database system capable of storing a great amount of measurement data taken at a short sampling interval over a long period of time.
2) No technique was provided for efficiently analyzing a vast amount of accumulated measurement data and quantitatively evaluating the operating conditions (3-dimensional distribution characteristics, non-steady phenomena, etc.) of a blast furnace based on the analysis.

The new system has been developed while taking advantage of the latest remarkable advancement in the computer technologies, wide availability of economical hardware and database systems capable of accumulating a vast amount of digital data and the enhancement and wider application of digital image processing technologies. The system incorporates as its foundation, the technologies to store a great amount of blast furnace operation data taken at as short a sampling interval as possible over a long time period and process the furnace operation data into visual information.

This paper outlines the following components of the developed system: the technology to process blast furnace operation data into visual information; the time differential ratio of stave cooler temperature calculated using a forgetting factor and the spatial differential vector of shaft pressure, which were newly defined as the products of secondary manipulations of the visual information; and the method of estimating and visualizing the position of the root of a cohesive zone by combining the above visual information products of the secondary manipulations.

2. Outline of Blast Furnace Process and Limitations of Conventional Analysis Techniques

A blast furnace is a moving-layer type counter-flow reaction vessel wherein: iron ore and coke, both in grains, are charged from its top one after the other so as to form a pile of their layers one over the other; hot air blast is blown in through blast injection nozzles (tuyeres) provided at its lower portion and the hot air makes the coke burn to generate high-temperature reduction gas; and iron oxide in the iron ore is reduced and melted by the high-temperature reduction gas into molten pig iron. This reaction vessel is a vertical, cylindrical pressure vessel having a larger diameter at the middle and composed of five sections, namely a throat, a shaft, a belly, a bosh and a hearth, in that order from top to bottom. The shaft and the bosh have a truncated cone shape (see **Fig. 1**[4]).

The tuyeres are provided in tens of units along the circumference

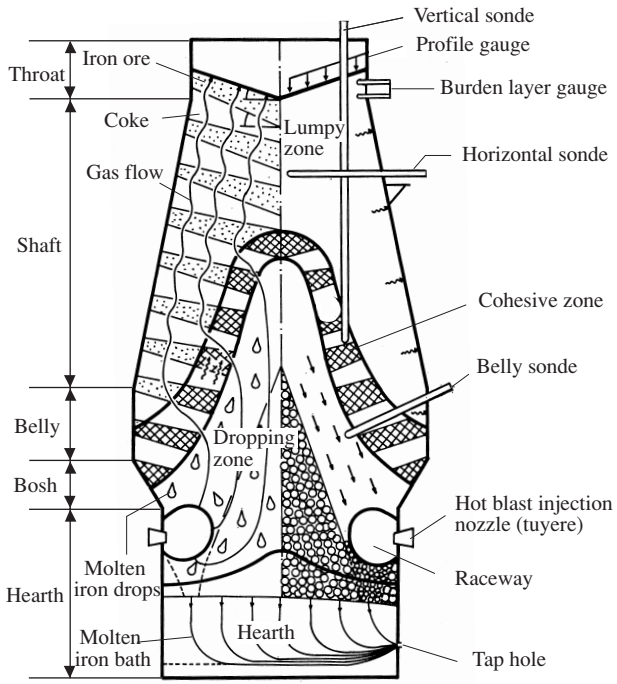

Fig. 1 Outline of blast furnace process[4]

of the furnace, and the air blown in through them at high temperature and pressure forms in front of them a space called raceway where coke in a coke-packed zone inside the tuyeres burns while moving spirally.

In the lumpy zone in the upper part of a blast furnace, the ore and coke charged from the furnace top gradually slide down as the charged materials are consumed in the lower part of the furnace, and in the meantime, the ore is heated and reduced by the reducing gas.

At the belly, as iron ore is heated and reduced, the viscosity of ore grains is lowered, they begin to soften and then fuse to form what is called a cohesive zone. Since the porosity of the fused ore grains is low, the permeability of the cohesive zone is also low. Thus, the cohesive zone has a structure in which layers of the low-permeability ore and those of the high-permeability coke (coke slits) are piled one over the other. This structure has been confirmed[12, 13] through past furnace interior investigations by furnace dissection[14-18] and probing with a belly sonde[19] or a deadman sonde[20].

In the dropping zone, which is the space just under the cohesive zone, molten metal and slag formed at the lower boundary of the cohesive zone drop down through a coke-packed layer and a central cone of coke called a deadman into a bath of molten iron in the hearth, molten slag floating on its surface. Then, the molten iron and slag are discharged to outside the furnace through a tap hole.

The gas flow in a blast furnace and the formation of the cohesive zone, which constitute factors essential for furnace operation, depend on the distribution of the ore/coke ratio in the radial direction. When the ore/coke distribution is adequately regulated by means of burden distribution control techniques, then the distribution of gas flow rate inside a blast furnace, the shape of the cohesive zone, the thermal loads near the furnace shell, etc. are appropriately controlled. Whether these are appropriately controlled can be judged by analyzing and evaluating the data from the temperature and pressure sensors provided at various positions of a furnace.

However, a blast furnace is a huge shaft furnace and the spatial

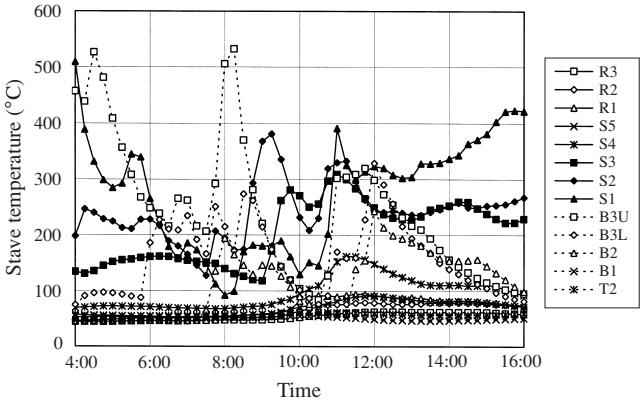

Fig. 2 Time trend of stave temperature distribution in furnace height direction (covering 180° of azimuthal angle)

distribution of phenomena that take place inside it varies not only in the radial direction but also in the vertical and circumferential (or azimuthal) directions. If measurement data from some sensors on a certain section of a blast furnace is analyzed simply in the form of a chart of independent time trends as shown in **Fig. 2**, for instance, the spatial distribution characteristics of blast furnace phenomena and their non-steady behaviors cannot be understood accurately.

3. Visual Evaluation and Numerical Analysis System of Blast Furnace

The developed system comprises 1) a database system to store measurement data, which are input to the process computer from many sensors from time to time over a long time period, in the form of digital data and 2) a software package to process the measurement data into visual information and apply secondary manipulations to the visual information on a personal computer (PC). The database system and the PC are connected to the process computer through a network to enable on-line data analysis. It is also possible by the system to extract any part of the accumulated digital data from the database system as required and analyze them off-line.

3.1 Technique to visualize blast furnace operation data[21, 22]

This technique is characterized by: visualizing the spatial distribution characteristics of measurement data from the sensors at various positions of a blast furnace in the form of 2-dimensional graphic information comprising isograms of the measurement data; and analyzing the time trends of the visualized data in the form of moving images.

Specifically, the process of the technique is as follows. The wall surface of a blast furnace is unfolded and projected onto a 2-dimensional plane where the ordinate and abscissa represent the height and circumference, respectively, of the furnace in question. The measurement data of each sensor is plotted on said plane at a position precisely corresponding to the position of the sensor from which the data came. Based on the above, an isogram chart comprising curves linking the positions having the same values of a measurement data item and a vector chart are generated. A virtual grid reflecting required spatial resolution is drawn covering the areas of the plane where no sensors are provided, and the value of a grid point is calculated by spatial interpolation based on the measurement data of the sensors located near the point and the actual 3-dimensional distances from these sensors.

The sensors are not necessarily distributed evenly on the projection plane and in order to cope with this, algorithms to carry out the spatial interpolation at high speed and draw isograms capable of dealing with any chosen sensor positions and realizing on-line analysis were developed.

Fig. 3 shows visualization examples of the temperature of staves

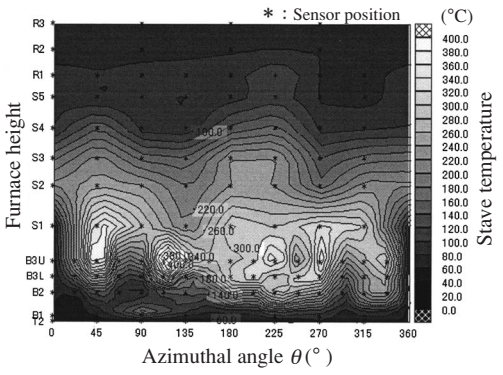

(a) Stave temperature

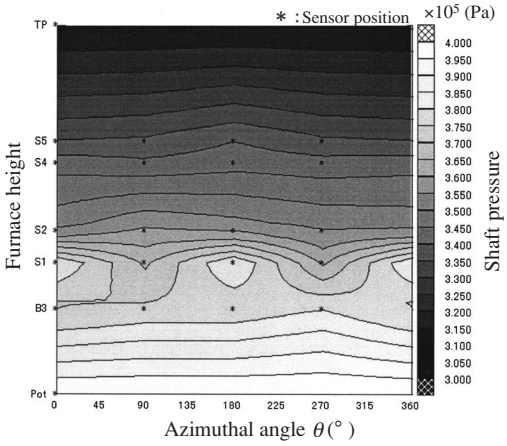

(b) Shaft pressure

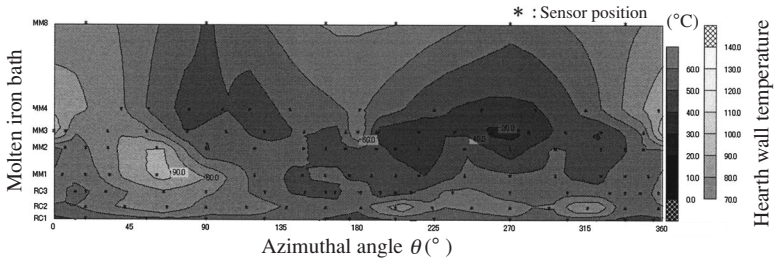

(c) Hearth wall temperature

Fig. 3 Visualization examples of stave temperature, shaft pressure and hearth wall temperature

covering the area of the shell of a blast furnace, the furnace inside pressure in its shaft and the temperature of its hearth wall. Note that, in relation to the above, the pressure in front of the tuyeres was estimated in consideration of the pressure loss from the hot-blast main to the blow pipes. When these visual images are renewed from time to time, the non-steady behaviors of the spatial distribution of the phenomena inside a blast furnace can be quantified and visually shown in the form of moving images.

As visualization examples corresponding to the time trend chart of Fig. 2, **Fig. 4** shows time trends of the distribution of stave temperature and shaft pressure in the furnace height direction.

3.2 Shape of cohesive zone and gas flow

As stated in section 2, the shape of the cohesive zone constitutes an important factor in controlling the gas flow inside a blast furnace. **Fig. 5** schematically shows examples of the cohesive zone shape and gas flow at the lower part of a blast furnace[19].

The cohesive zone shape of Fig. 5 a) is called an inverse V shape. In this case, the dropping zone is tall and the root of the cohesive zone near the furnace wall is sufficiently away from the raceway and as a consequence, the flow of the hot blast blown in through the tuyeres forms dominantly a central gas flow ①. Here, a part of the central gas flow ① branched out to form a cohesive zone coke slit gas flow ② and then, getting together with a dropping zone peripheral gas flow ③, forms a lumpy zone peripheral gas flow ④.

The cohesive zone shape of Fig. 5 b), on the other hand, is called a W shape. This type of cohesive zone forms, for example, when the ore/coke ratio is high at the middle of furnace radius and the portion of the cohesive zone corresponding to the zone of the high ore/coke ratio, where the reduction reaction goes slower, falls to near the inner part of the raceway. In this case, it is presumed that the flow of

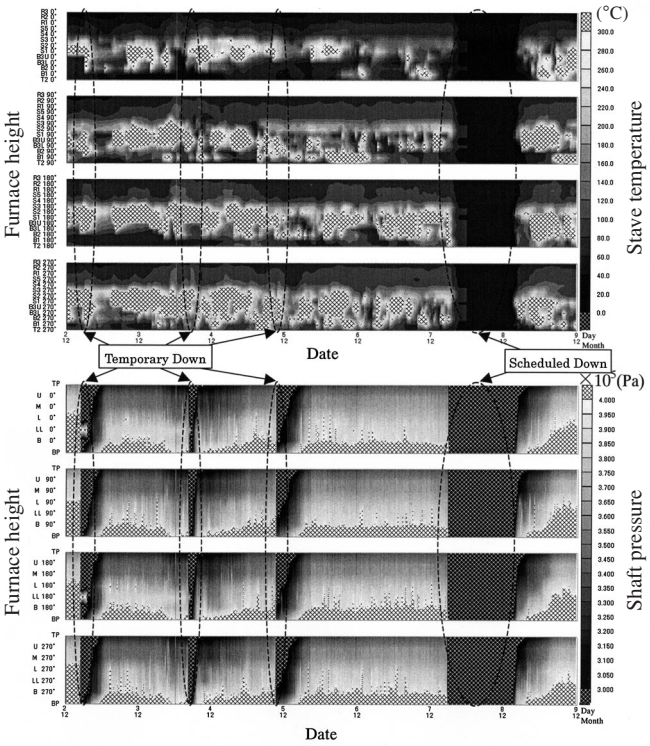

Fig. 4 Time trends of height direction distribution of stave temperature and shaft pressure

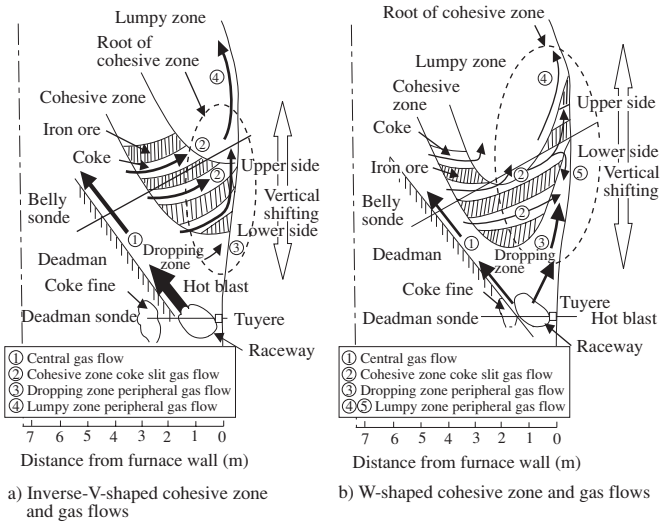

Fig. 5 Shapes of cohesive zone and gas flows

the hot blast from the tuyeres toward the furnace center is decreased, a considerable part of the hot blast flows toward the furnace wall and as a result, a dropping zone peripheral gas flow ③ develops, causing the cohesive zone root near the furnace wall to rise toward the furnace top.

The position of the whole cohesive zone shifts vertically during furnace operation as shown with white arrows in Fig. 5 depending on the conditions of furnace operation and burden distribution and its shape and position vary also circumferentially for various reasons. In such a situation, it is important for furnace operation control to estimate the vertical position, thickness and shape of the cohesive zone, especially the circumferential distribution of these properties.

The visualized data of the spatial distributions of stave temperature and shaft pressure shown in Figs. 3 and 4 are considered to reflect the shape of the cohesive zone, namely the level, thickness and shape of its root, near the furnace wall. Based on the above understanding of the phenomena inside a blast furnace, the authors studied to work out a technique to estimate and visualize the cohesive zone root by applying a secondary manipulation to the visualized data.

3.3 Time differential ratio of stave temperature with forgetting factor[23]

The permeability of a cohesive zone is low and for this reason, if its thickness and shape are uneven in the circumferential direction, the gas does not flow through it homogeneously and local gas passages form at its portions of smaller gas-flow resistance; this is considered to occur with relatively high frequency. It is suspected that if this takes place, the time fluctuation of stave temperature is greater near the region where there is such a local and selective gas passage than in other regions. On this assumption, the time differential ratio of stave temperature was selected as the item of a secondary manipulation of the visual information data, and the time fluctuation was visually projected onto a 2-dimensional plane having coordinates of furnace height and circumferential (azimuthal) position (see **Fig. 6**). As a result, regions which had been intuitively assumed to correspond to the root of a cohesive zone were distinguished as the regions showing larger time fluctuations of stave temperature (the hatched areas in Fig. 6).

In the above, the stave thermometers were not directly measuring the temperature inside the furnace but that of staves. In consider-

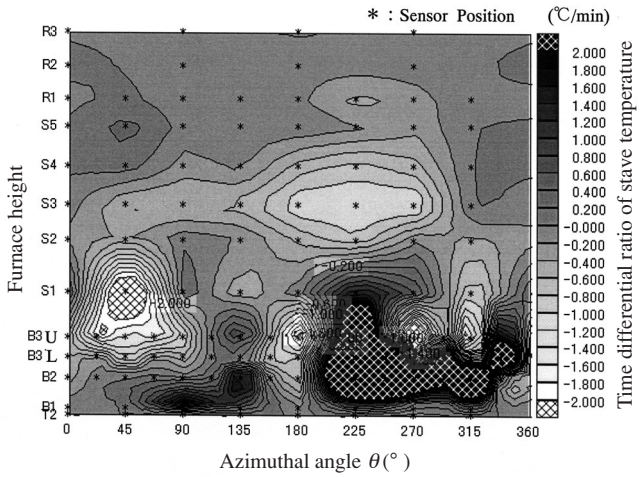

Fig. 6 Spatial distribution of time differential ratios of stave temperature with forgetting factor

ation of the influence of the heat capacity of a furnace wall including staves, a time differential ratio based on a forgetting type moving average standard and using an exponential function as the weighting coefficient was introduced, as shown in Equation (1), as the time differential ratio $\Delta T_{(h,r,\theta,t)}$ of the temperature of a stave at a position of height h, furnace radius r and azimuthal angle θ at time t.

$$\Delta T_{(h,r,\theta,t)} = \left[T_{(h,r,\theta,t)} - \frac{\sum_{k=1}^{n} \rho^{(-m\cdot k\cdot \Delta t)} \cdot T_{(h,r,\theta,t-m\cdot k\cdot \Delta t)}}{\sum_{k=1}^{n} \rho^{(-m\cdot k\cdot \Delta t)}} \right] \div (m\cdot \Delta t)\ (\mathrm{^\circ C/min}) \quad \cdots\cdots (1)$$

where, ρ is a forgetting factor (-) (ρ > 1),
Δt is sampling time (min),
n is the number of data evaluated (-),
m is the number of standard time (-), and
k is a discrete time counter counting back to the past (-) (k = 1, 2, ···, n).

Note that the time of the stave temperature condition shown in Fig. 6 is the same as that of Fig. 3 (the same applies also to the figures presented hereafter). In addition, a forgetting-type, moving-average time differential ratio was calculated with respect to the stave temperature data of the last 20 min on the following assumptions: ρ = 1.4 (-), Δt = 1 (min), n = 4 (-), and m = 5 (-).

3.4 Spatial differential vector of shaft pressure[23)]

The position of a cohesive zone has long been estimated based on shaft pressure distribution on account of its higher gas-flow resistance[24)]. With respect to this, the authors attempted to estimate the positions of the upper and lower boundaries of the cohesive zone root using the spatial differential vector of shaft pressure defined by its 3-dimensional distribution.

At the upper side of the cohesive zone root in Fig. 5, the upward flow of the lumpy zone peripheral gas flow ④ is presumed to be strong because the cohesive zone coke slit gas flow ② joins with it there. At the lower side of the root, on the other hand, the resistance to an upward gas flow along the furnace wall is large and, in the case of a W-shaped cohesive zone as shown in Fig. 5 b), the upward gas flow along the furnace wall is considered to be weak, because it is presumably hindered by a downward flow ⑤ that has passed through the cohesive zone.

On this assumption, the spatial differential vector of shaft pressure, which corresponds to gas flows, was selected as the item of a secondary manipulation of the visual information data, and its spatial distribution was visually projected onto a 2-dimensional plane having coordinates of furnace height and azimuthal position (see **Fig. 7**). As a result, the upper side of the region which had been considered to correspond to the upper side of the cohesive zone root was distinguished as a region showing a large vector (the areas of white hatching in Fig. 7) and a small angle of deflection, and its lower side as a region showing a small vector and a large angle of deflection.

Here, the spatial differential vector of shaft pressure $\vec{p}_{spv\,(h,r,\theta,t)}$ was defined in consideration of the vertical shaft furnace shape having a larger diameter at the middle. That is, using the shaft pressure $P_{(h,r,\theta,t)}$(Pa) at the position "a" (height h, furnace radius r, azimuthal angle θ at time t) and a tangential plane "A" at the position "a" having a height tangential axis y and a circumferential tangential axis l (see **Fig. 8**), the above vector was defined as a vector including, as a

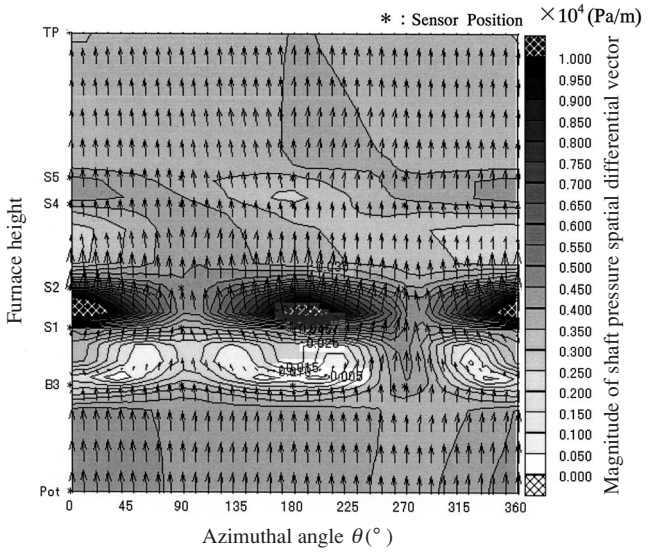

Fig. 7 Spatial distribution of spatial differential vector of shaft pressure

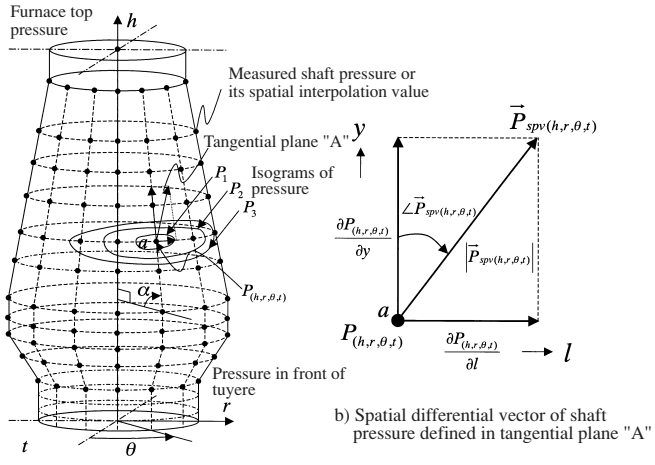

Fig. 8 Definition of spatial differential vector of shaft pressure

component, the partial differential coefficient of the shaft pressure $P_{(h,r,\theta,t)}$ at the position "a" as in Equations (2) to (4) below, and with this the measurement data were visualized and expressed in the form of a vector chart.

$$\vec{p}_{spv\,(h,r,\theta,t)} = \left(\frac{\partial P_{(h,r,\theta,t)}}{\partial l}, \frac{\partial P_{(h,r,\theta,t)}}{\partial y} \right) \quad \cdots\cdots (2)$$

1) The magnitude of the spatial differential vector of shaft pressure

$$\left| \vec{P}_{spv\,(h,r,\theta,t)} \right| = \sqrt{ \left(\frac{\partial P_{(h,r,\theta,t)}}{\partial l} \right)^2 + \left(\frac{\partial P_{(h,r,\theta,t)}}{\partial y} \right)^2 } \ \text{(Pa/m)} \quad \cdots\cdots (3)$$

2) The angle of deflection of the spatial differential vector of shaft pressure

$$\angle \vec{P}_{spv\,(h,r,\theta,t)} = \tan^{-1} \left(\frac{\dfrac{\partial P_{(h,r,\theta,t)}}{\partial l}}{\dfrac{\partial P_{(h,r,\theta,t)}}{\partial y}} \right) (^\circ) \quad \cdots\cdots (4)$$

where, the angle is defined as being positive in the clockwise direction about the height tangential axis y.

$$-180\,(^\circ) < \angle \vec{P}_{spv\,(h,r,\theta,t)} \leq +180\,(^\circ)$$

Note that the magnitude of the vector $\left| \vec{P}_{spv\,(h,r,\theta,t)} \right|$ corresponds to a spatial expansion of the conventional indicator of shaft pressure drop $\frac{\Delta P}{L}$(Pa/m).

3.5 Method of estimating and visualizing cohesive zone root by center of gravity identification method

It is suspected that the time differential ratio of stave temperature is large at the root of a cohesive zone as shown in Fig. 6. It is also suspected that the magnitude of spatial differential vector of shaft pressure is large and its angle of deflection small at the upper side of the cohesive zone root, and that the magnitude of the vector is small and its angle of deflection large at the lower side, as shown in Fig. 7.

Based on the above assumption, the authors worked out a method of estimating and visualizing the circumferential distribution of the positions of the upper and lower boundaries of the cohesive zone root. This is done as follows: threshold values of these items are determined; figure zones delineated by the isograms of the threshold values are cut out; the contours of the cut-out figure zones are divided into upper and lower curves; and the upper and lower curves are averaged.

Examples of the threshold values for a blast furnace equipped with cast iron staves are listed in **Table 1**, and an example of a chart comprising figure zones delineated by the isograms of the threshold values is given in **Fig. 9**.

Here, it is assumed that, at an azimuthal angle θ (°), the root of a cohesive zone exists in the region between an upper boundary height $U_{(\theta)}$ (m) and a lower boundary height $L_{(\theta)}$ (m), and that the center of gravity in the furnace height direction $G_{(\theta)}$ (m) of the cohesive zone root coincides with the average center of gravity $\overline{G}_{(\theta)}$ (m) of the above-said region. That is to say, by this center of gravity identification method, $U_{(\theta)}$ and $L_{(\theta)}$ are calculated using Equations (5) and (6) by the weighted average method.

Table 1 Examples of threshold values

Magnitude of spatial differential vector of shaft pressure	Upper threshold value $\left\vert \vec{P}_{spv} \right\vert_{UTH}$	8 kPa/m
	Lower threshold value $\left\vert \vec{P}_{spv} \right\vert_{LTH}$	1 kPa/m
Angle of deflection of spatial differential vector of shaft pressure	Threshold value $\left\vert \angle \vec{P}_{spv} \right\vert_{TH}$	90°
Time differential ratio of stave temperature with forgetting factor	Upper threshold value $\dot{T}_{UTH}$	+ 0.8°C/min
	Lower threshold value $\dot{T}_{LTH}$	– 0.8°C/min
Stave temperature	Upper threshold value T_{UTH}	320°C
	Lower threshold value T_{LTH}	180°C

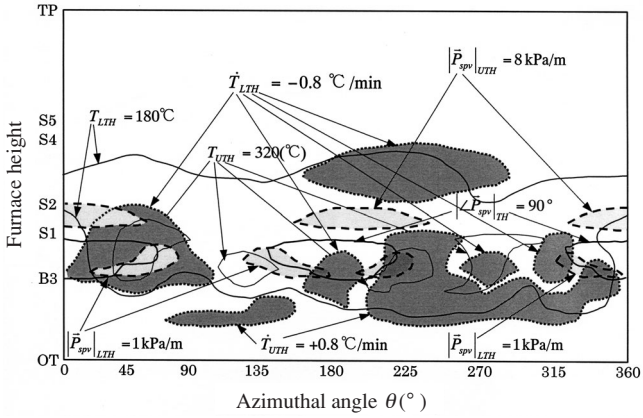

Fig. 9 Example of figure zones delineated by threshold isograms

$$U_{(\theta)} = \frac{\sum_{i=1}^{N_{1(\theta)}} w_1 \cdot \left(h^U_{1i(\theta)} + h^L_{1i(\theta)} \right)}{\sum_{i=1}^{N_{1(\theta)}} w_1} + \frac{\sum_{j=4}^{7} \sum_{i=1}^{N_{j(\theta)}} \left(w_j \cdot h^U_{ji(\theta)} \right)}{\sum_{j=4}^{7} \sum_{i=1}^{N_{j(\theta)}} w_j} \quad \cdots\cdots (5)$$

$$L_{(\theta)} = \frac{\sum_{j=2}^{3} \sum_{i=1}^{N_{j(\theta)}} w_j \cdot \left(h^U_{ji(\theta)} + h^L_{ji(\theta)} \right)}{\sum_{j=2}^{3} \sum_{i=1}^{N_{j(\theta)}} w_j} + \frac{\sum_{j=4}^{7} \sum_{i=1}^{N_{j(\theta)}} \left(w_j \cdot h^L_{ji(\theta)} \right)}{\sum_{j=4}^{7} \sum_{i=1}^{N_{j(\theta)}} w_j} \quad \cdots\cdots (6)$$

provided $L_{(\theta)} < U_{(\theta)} \leq h^U_{7i(\theta)}$ $\cdots\cdots (7)$

where, $h^U_{ji(\theta)}$ is the upper curve of figure zone species j (m),

$h^L_{ji(\theta)}$ is the lower curve of figure zone species j (m),

$N_{j(\theta)}$ is the number of the figure zone species j existing at azimuthal angle θ (-),

i is the counter of the figure zone species j existing at azimuthal angle θ (-), and

w_j is the weighting coefficient of the figure zone species j (-).

The first terms of Equations (5) and (6) relate to the magnitude and angle of deflection of the spatial differential vector of shaft pres-

sure, and their second terms relate to stave temperature and its time differential ratio. Equation (7) was used as a restricting condition.

Equation (8) below is obtained by adding both the sides of Equations (5) and (6) and dividing by 2.

$$G_{(\theta)} = \overline{G}_{(\theta)} \quad \cdots\cdots (8)$$

Table 2 shows the relationship between the threshold values, the figure zone species (j = 1, 2, ···, 7) and the upper and lower curves,

Table 2 Relationship between threshold values, figure zone species and upper and lower curves

Furnace height coordinates of divided contours of figure zone $h_{(\theta)}$(m)		Upper curve	Lower curve
Magnitude of spatial differential vector of shaft pressure	Upper threshold value	$h^{U}_{1i(\theta)} = \left\vert \vec{P}_{spv} \right\vert^{U}_{UTH(\theta)i}$	$h^{L}_{1i(\theta)} = \left\vert \vec{P}_{spv} \right\vert^{L}_{UTH(\theta)i}$
	Lower threshold value	$h^{U}_{2i(\theta)} = \left\vert \vec{P}_{spv} \right\vert^{U}_{LTH(\theta)i}$	$h^{L}_{2i(\theta)} = \left\vert \vec{P}_{spv} \right\vert^{L}_{LTH(\theta)i}$
Angle of deflection of spatial differential vector of shaft pressure	Threshold value	$h^{U}_{3i(\theta)} = \left\vert \angle \vec{P}_{spv} \right\vert^{U}_{TH(\theta)i}$	$h^{L}_{3i(\theta)} = \left\vert \angle \vec{P}_{spv} \right\vert^{L}_{TH(\theta)i}$
Time differential ratio of stave temperature with forgetting factor	Upper threshold value	$h^{U}_{4i(\theta)} = \dot{T}^{U}_{UTH(\theta)i}$	$h^{L}_{4i(\theta)} = \dot{T}^{L}_{UTH(\theta)i}$
	Lower threshold value	$h^{U}_{5i(\theta)} = \dot{T}^{U}_{LTH(\theta)i}$	$h^{L}_{5i(\theta)} = \dot{T}^{L}_{LTH(\theta)i}$
Stave temperature	Upper threshold value	$h^{U}_{6i(\theta)} = T^{U}_{UTH(\theta)i}$	$h^{L}_{6i(\theta)} = T^{L}_{UTH(\theta)i}$
	Lower threshold value	$h^{U}_{7i(\theta)} = T^{U}_{LTH(\theta)i}$	$h^{L}_{7i(\theta)} = T^{L}_{LTH(\theta)i}$

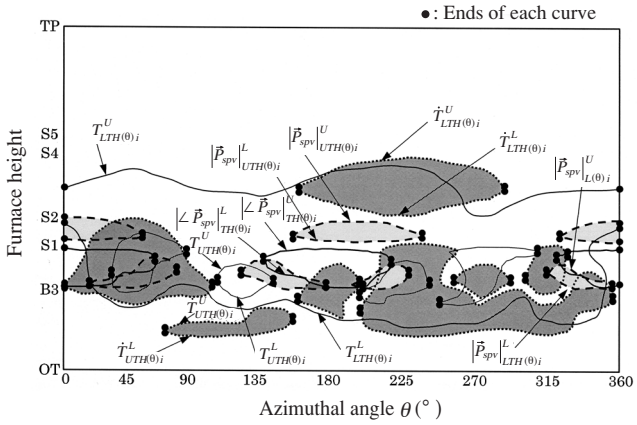

Fig. 10 Examples of upper and lower curves of figure zones

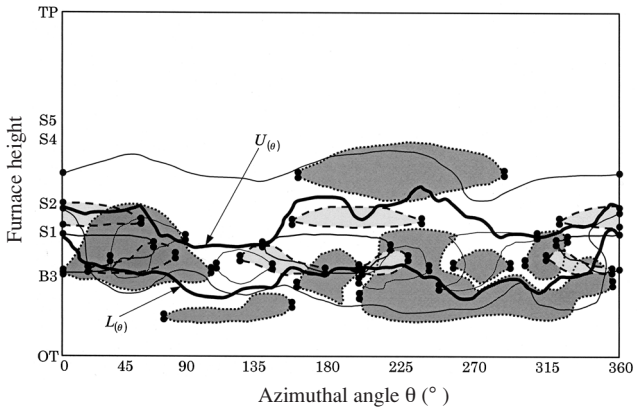

Fig. 11 Example of estimation and visualization of cohesive zone root

Fig. 10 examples of the upper and lower curves of figure zones, and **Fig. 11** an example of the estimation and visualization of the root of a cohesive zone. Here, all the weighting coefficients w_j were set equal to 1.0 (w_j = 1.0, j = 1, 2, ···, 7) so as to equalize the contributions of all the figure zone species. As seen in Fig. 11, a good overview of blast furnace operation is obtained when the non-steady behaviors in the time fluctuations of measurement data are analyzed in correlation with operation conditions.

The threshold values and weighting coefficients will be further verified through examination referring to the results of actual furnace operation and calculations using physical model simulators[25].

4. Closing

The image of whole operation condition of a blast furnace, which had so far been conjectured, relying on the reasoning of experienced furnace operators, based on measurement data at a certain instant and charts of their time trends, came to be shown in the form of objective visual information as a result of the development of the visual evaluation and numerical analysis system of blast furnace. The developed system made it possible to quantitatively evaluate the non-steady behaviors of spatial distribution of phenomena inside a blast furnace, and has been applied to the operation supervision of commercial blast furnaces.

The developed system made it clear that important blast furnace operation control information, which had been latent in furnace measurement data, such as the circumferential distribution of the root of a cohesive zone could be visually elicited by applying secondary manipulations, temporally and spatially, to visualized information of the measurement data.

The authors intend further to develop, by verifying the effectiveness of the developed system through application to actual furnace operation, a technique to quantitatively evaluate non-steady behaviors of phenomena inside a blast furnace, which show spatial distribution of their characteristics, and a new modeling technique and a system for it capable of proposing operation guidance flexibly and adequately.

References

1) Yagi, J.: Tetsu-to-Hagané. 69(10), 1242(1983)
2) Takatani, K.: Tetsu-to-Hagané. 81(11), 1031(1995)
3) Nogami, H.: Tetsu-to-Hagané. 89(2), 211(2003)
4) Sugiyama, T., Sugata, M.: Seitetsu Kenkyu. (325), 34(1987)
5) Yagi, J., Akiyama, T.: CAMP-ISIJ. 2, 2(1989)
6) Yamazaki, Sato, Kiguchi, Iida, Fukumura: CAMP-ISIJ. 2, 6(1989)
7) Nagai, Arai, Matsuda, Kadoguchi, Yabata: CAMP-ISIJ. 2, 10(1989)
8) Ohtsuka, Matsuoka, Aminaga, Yoshida, Yokoi, Inada: CAMP-ISIJ. 2, 14(1989)
9) Takarabe, Nakamori, Oda, Taira, Watanabe, Seki: CAMP-ISIJ. 2, 18(1989)
10) Niwa, Sumikame, Sakurai, Aoki: CAMP-ISIJ. 2, 22(1989)
11) Takatani, K., Inada, T., Ujisawa, Y.: ISIJ Int. 39(1), 15(1999)
12) Wakuri, Morishita, Ashimura, Inoue, Hirata, Sugiyama: Tetsu-to-Hagané. 72, A9(1986)
13) Ashimura, Morishita, Inoue, Higuchi, Baba, Kanamori, Wakuri: Tetsu-to-Hagané. 80(6), 457(1994)
14) Kambara, Hagiwara, Shigemi, Kondo, Kanayama, Wakabayashi, Hiramoto: Tetsu-to-Hagané. 62(5), 535(1976)
15) Shimomura, Nishikawa, Arino, Katayama, Hida, Isoyama: Tetsu-to-Hagané. 62(5), 547(1976)
16) Sasaki, Ono, Suzuki, Okuno, Yoshizawa, Nakamura: Tetsu-to-Hagané. 62(5), 559(1976)
17) Kojima, Nishi, Yamaguchi, Nakama, Ida: Tetsu-to-Hagané. 62(5), 570(1976)
18) Joint Committee for Iron- and Coke-making of ISIJ: Progress of Iron-making Technologies in Japan (Special Report No. 24). ISIJ, May 1977, p.49-52

19) Wakuri, Kanamori, Higuchi, Doi, Miyabe: Tetsu-to-Hagané. 69, S83(1983)
20) Wakuri, Mochizuki, Inoue, Hirata, Higuchi, Tamura: Tetsu-to-Hagané. 71, S62(1985)
21) Ito, M., Matsuzaki, S.: CAMP-ISIJ. 15, 927(2002)
22) Matsuzaki, S., Ito, M.: CAMP-ISIJ. 15, 928(2002)
23) Ito, M., Matsuzaki, S.: CAMP-ISIJ. 16, 300(2003)
24) Kase. M., Sugata, M., Yamaguchi, K.: Tetsu-to-Hagané. 66(13), 1928(1980)
25) Naito, M., Nishimura, T.:Asia Steel International Conference 2000. Vol.B(Ironmaking), 2000, p.268